Fate and transport of chromium in industrial sites: dynamic simulation on soil profile

Yan, X.; Yang, B.; He, E.; Peijnenburg, W.J.G.M.; Zhao, L.; Xu, X.; ... ; Qiu, H.

Science of the Total Environment 858 (2023) 159799

Contents lists available at ScienceDirect

Science of the Total Environment

journal homepage: www.elsevier.com/locate/scitotenv

Fate and transport of chromium in industrial sites: Dynamic simulation on soil profile

Xuchen Yan [a], Bin Yang [a], Erkai He [b], Willie J.G.M. Peijnenburg [c,d], Ling Zhao [a], Xiaoyun Xu [a], Xinde Cao [a], Ana Romero-Freire [e], Hao Qiu [a,*]

[a] School of Environmental Science and Engineering, Shanghai Jiao Tong University, Shanghai 200240, China
[b] School of Geographic Sciences, East China Normal University, Shanghai 200241, China
[c] Institute of Environmental Sciences, Leiden University, Leiden 2333CC, the Netherlands
[d] National Institute of Public Health and the Environment, Center for the Safety of Substances and Products, Bilthoven 3720BA, the Netherlands
[e] Department of Soil Science, University of Granada, Granada 18002, Spain

HIGHLIGHTS

- Soil pH and Fe content significantly affected Cr(VI) migration and transformation.
- Heterogeneous soil profiles were constructed to reflect the vertical migration of Cr.
- A long-term risk assessments model of Cr vertical migration was developed.

GRAPHICAL ABSTRACT

ARTICLE INFO

Editor: Deyi Hou

Keywords:
Cr
Transport
Soil profile
Industrial sites
Dynamic simulation

ABSTRACT

Direct discharge of chromium-containing waste water and improper disposal of waste residues in industrial sites may lead to the vertical migration of metals into aquifers, posing serious threat to soil-groundwater system. The heterogeneity in soil profile further aggravates the complexity and unpredictability of this transport process. However, topsoil was the main focus of most studies. Herein, the vertical transport and transformation of Cr in soils at different depths in three industrial sites (i.e., Shijiazhuang, Zhuzhou, and Guangzhou) were investigated to delineate Cr transport and retention characteristics under complex conditions. Regional and vertical differences in soil properties led to the specificity in Cr migration behaviors among these three sites. Correlation analysis showed that soil pH ($r = -0.909$, $p < 0.05$) and Fe content ($r = 0.949$, $p < 0.01$) were the major controlling factors of Cr(VI) migration and transformation in aquifers. Furthermore, the soil of Zhuzhou site showed the maximum adsorption capacity for Cr(VI) (0.225 mol/kg), and the strongest reduction ability of Cr(VI) was observed in the Guangzhou soil. Results of model-based long-term forecast indicated that the Cr(III) concentration in the liquid phase of Guangzhou subsoil could reach 0.08 mol/m^3 within 20 years. Heavier rainfall condition exacerbated the contamination due to an increased pollutant flux and enhanced convection. Specially, Cr was fixed in the topsoil of Zhuzhou site with the formation of $PbCrO_4$ and presented least vertical migration risk. The conclusions above can provide scientific theoretical guidance for heavy metal pollution prevention and control in industrial contaminated regions.

* Corresponding author.
E-mail address: haoqiu@sjtu.edu.cn (H. Qiu).

http://dx.doi.org/10.1016/j.scitotenv.2022.159799
Received 31 May 2022; Received in revised form 24 October 2022; Accepted 24 October 2022
Available online 27 October 2022

1. Introduction

Soil quality and safety play an important role in maintaining socioeconomic development and ensuring human health (Liu et al., 2022). However, soil heavy metal pollution is becoming increasingly prominent due to the rapid industrialization worldwide, especially in industrial areas relating to mining, metal processing and smelting, fossil fuel combustion, chemical production and industrial emissions (Balkhair, 2017; Parizanganeh et al., 2010; Qiu et al., 2022). Due to the accumulation of persistent heavy metals, contaminant concentrations in soils of industrial sites may by far exceed environmental standards. Furthermore, the range of the polluted soil area would expand with the transport of metals as a function of rainfall and flow field, and thus endangering soil ecosystem functioning and threatening the wellness of human beings (Xiao et al., 2015).

Cr is a common toxic soil contaminant (Liang et al., 2021) which is discharged into the soil environment in large quantities through industrial processes such as paper making, wood processing (del Real et al., 2020) and dye production (Tumolo et al., 2020). It has been estimated that 1.29 million tons of Cr are released into the environment per year, resulting in serious soil metal pollution (Coetzee et al., 2020). Cr in soil commonly exists in its trivalent and hexavalent states, which differ in chemical properties and mobility (Chen et al., 2018). Cr(III) readily binds to iron oxides and eventually exists as chromite or silicate minerals in soil (Ao et al., 2022b). Compared with Cr(III), Cr(VI) in the forms of CrO_4^{2-}, $HCrO_4^-$ and $Cr_2O_7^{2-}$ has a stronger transport tendency owing to its high solubility in pore water (Megremi et al., 2019). Therefore, Cr in different forms displays quite different environmental behaviors, resulting in substantial differences in environmental impacts. Cr can transform between the two valence states during migration. This transformation has received less attention (Lov et al., 2017). However, accurate estimation of the risk of Cr pollution during the expansion of its pollution range largely depends on the transformation dynamics of Cr. These transformation dynamics require detailed investigation.

Metals tend to migrate vertically to deeper horizons rather than being retained in topsoil under the leakage of sewage, percolation of solid residues and surface runoff by rainfall (Li et al., 2009; Peng et al., 2022; Zhu et al., 2019). Cr(VI) tends to be retained by clay layers, and the concentration of Cr(VI) and total Cr was found to reach its maximum at a soil depth of 5– 10 m, which can extend to tens of meters after years of accumulation (Wang et al., 2020a). Previous studies have verified that Cr can accumulate extensively in deep soils of rapidly industrializing regions, which would be a potential environmental problem (Bai et al., 2011; Li et al., 2009; Wu et al., 2010; Zhu et al., 2019). Moreover, chromium residues can transport through the vadose zone into the groundwater. The crystalline structure of Cr(III) bounded to minerals is quite unstable and susceptible to dissolution. This process can lead to further longitudinal migration of contamination (Sedlazeck et al., 2017). In the surrounding area of lignite power plants, the diffusion of fly ash may also cause groundwater pollution of Cr under the action of local leaching which can be as high as 120 $\mu g \cdot L^{-1}$ (Izbicki et al., 2015). Soil is a highly heterogeneous medium with different structures and properties at each soil horizon. This results in complex vertical migration behavior of metals. Currently, most studies on substance migration remain narrow in focus of homogeneous soils (Balkhair, 2017; Dinter et al., 2021; Lov et al., 2017; Yang et al., 2022), which hinders to decipher the mechanism of vertical migration of Cr in porous media. Thus, taking account of heterogeneous soil profiles with a depth up to 6 m in this study is more suited to model real scenarios of the vertical migration behavior of metals in soil.

Soil properties such as redox potential, pH and presence of soil minerals are the key factors affecting the fate of Cr in soils (Choppala et al., 2018). In general, the adsorption of Cr(VI) on soil increases with lower pH (Jardine et al., 2013) whereas the retention of Cr(III) in soil increases with increasing pH (Choppala et al., 2018). Under the condition of pH < 6, Cr(VI) is attached to cationic colloids such as FeO(OH) and Al_2O_3 through electrostatic adsorption or hydrogen bond formation (Liang et al., 2021; Richard and Bourg, 1991). The presence of competing oxygen anions and compounds may restrict Cr(VI) adsorption (Namiesnik and Rabajczyk, 2012). Additionally, Cr adsorption is positively correlated with the total organic carbon (TOC) content due to the high positive charge on the cationic colloids (Banks et al., 2006; Wang et al., 2020b). This can further inhibit Cr mobility (Zeng et al., 2011). Reductive soil components such as Fe(II) minerals, sulfide and organic matter can also participate in the chemical reduction of Cr(VI) (Li et al., 2020), so as to affect the transformation and migration of Cr. The adsorption, migration, and transformation processes of metals in soil are highly interlinked and often occur synchronously, further enhancing the complexity of the coupling mechanism of metal migration and diffusion. The complicated interactions among soil properties may thus hinder our comprehension of the mechanisms of Cr migration. Representative industrial sites with characteristic soil properties could allow to develop excellent models to elucidate the process determining the fate of Cr in industrial soils. Furthermore, the regional differences in geological structure and hydrological characteristics could also lead to different transport and transformation behavior of Cr in soils. Due to the extensive distribution of industrial sites in China, scholars have not conducted systematic studies of Cr transfer and transformation in different regional soils.

Shijiazhuang, Zhuzhou, and Guangzhou are situated in typical industrialized regions of Beijing-Tianjin-Hebei, Changsha-Zhuzhou-Xiangtan, and Pearl River Delta, respectively, with frequent industrial activities, where the soils are much more likely to be contaminated with heavy metals than in other regions. Moreover, the geological structure and soil physicochemical properties of these representative areas exhibited significant regional differences. Against this background, we collected the soil samples from a chemical site in Shijiazhuang, a smelting site in Zhuzhou, and a mechanical processing site in Guangzhou to explore the influence of soil components and physicochemical properties on Cr migration in view of regional representativeness in geohydrological and industry characteristics. Various depths of soils from three representative industrial sites were selected to illuminate the migration and transformation processes of Cr in the heterogeneous soil profiles. Furthermore, we proposed a modeling method based on the soil structures of actual sites to simulate vertical migration and diffusion of Cr in soil profiles and predict the long-term risks of Cr migration in industrial sites. The specific aims of the study are as follows: (1) to describe the one-dimensional migration behavior of Cr in soil columns at different soil depths and determine the influence of soil textures; (2) to reveal the effect of soil structures and properties on Cr(VI) vertical transport and transformation in different industrial sites; (3) to study the fate of Cr in soil profile systems and assess the risks associated with long-term vertical transport of Cr in three industrial sites. Considering the heterogeneity in soil profiles and the uniqueness of regional geological conditions, we carried out researches on the transport and transformation of Cr at a deeper and larger scale, which can better reflect the fate of Cr in soils. This work can provide a scientific theoretical basis for Cr transport and transformation in soils under realistic scenarios. Moreover, the longitudinal migration model presented in this study can be used to predict the Cr transport in high-risk industrial areas and offer support for pollution prevention and remediation of industrial sites.

2. Materials and methods

2.1. Soils and chemicals

Soil samples were collected at two depths (1– 3 m and 4– 6 m) from industrial sites in Shijiazhuang (H), Zhuzhou (Z) and Guangzhou (G), China, on account of the property difference in soil profile, contamination status, and geological conditions in these representative regions. According to the sampling depth, soil samples were divided into groups of 1– 3 m and 4– 6 m, which were denoted by the numbers 1 and 2 respectively. The soils in each horizon possess similar physical and chemical properties. After being mixed evenly, soil samples of the same depth were air-dried, ground and sieved to obtain soil aggregates with uniform particle size range (600– 710 μm) (Chen et al., 2019). The primary physicochemical properties of the soils from the different regions are presented in Table 1.

Table 1
The physicochemical properties of multi-horizon soils in three regions.

Soils[a]	Texture	Clay (%)	Sand (%)	Silt (%)	pH	TOC (mg/g)	DOC (mg/kg)	CEC (cmol/kg)	Al (mg/g)	Ca (mg/g)	Fe (mg/g)	Mn (mg/g)	Pb (mg/g)
H1	Silt loam	7.0	18.7	74.3	8.2	30.22	13.95	33.65	36.93	12.57	27.27	0.38	52.11
H2	Sandy loam	1.5	66.9	32.6	8.6	5.76	7.98	3.63	53.07	11.61	27.59	0.27	56.63
Z1	Silt loam	12.2	37.2	50.7	5.1	11.68	96.30	14.91	11.41	5.83	99.49	0.74	2.59E+4
Z2	Silt loam	5.4	31.1	63.5	4.5	28.82	80.63	13.81	13.17	0.69	72.80	0.53	201.71
G1	Silt loam	4.3	43.4	52.4	7.5	29.67	102.18	12.33	13.65	3.67	30.88	0.31	42.63
G2	Sandy loam	3.0	47.2	49.8	7.3	34.35	97.50	9.71	13.87	0.57	33.48	0.24	42.51

[a] Letter represents different industrial sites (H: Shijiazhuang; Z: Zhuzhou; G: Guangzhou), and number indicates the depth of the soil horizon (1:1– 3 m; 2: 4– 6 m). TOC indicates total organic carbon, DOC indicates dissolved carbon, and CEC indicates cation exchange capacity.

A chromium containing solution was prepared by dissolving analytical grade K_2CrO_4 powder (Sigma-Aldrich Co., Ltd. D.) in deionized water. The concentration of Cr in the influent used for column experiments was set at 10 mg/L, as based on previously reported data (Muthukumaran and Beulah, 2010).

2.2. Column experiments

Transport experiments were conducted in columns made of borosilicate glass. The inner diameter of the device was set to 1.2 cm, and the soil filling height was 8 cm according to a previous study (Chen et al., 2019; Jia et al., 2017).

In the homogeneous column experiments, different soils were dry-packed into the columns individually to subsequently simulate the transport of contaminants in a single soil horizon. Detailed column filling parameters are shown in Table S1. Peristaltic pumps (BT100-2J, Longer Precision Pump Co., Ltd., China) were employed to achieve a steady up-flow field. Before the injection of a Cr-containing solution, the column was saturated with up to 50 pore volumes (PVs) deionized water with a flow rate of 0.23 cm/min. A Cr-containing solution with a concentration of 10 mg/L was pumped into the column afterwards to simulate the sewage infiltration process. During the transport, effluents were collected continuously in glass tubes at regular time intervals (one PV each time) via an automatic fraction collector (BS-100A, Huxi Analytical Instrument Factory Co., Ltd., China). Each treatment had three replicates. Soil samples were excavated in two fractions by height for each column as the transport experiment was finished.

Multi-horizon column experiments were further conducted to simulate the longitudinal soil heterogeneity in industrial sites. Two soils collected at different depths were filled into the column in sequence according to their distribution in the soil profiles. For sites in Shijiazhuang and Guangzhou, the filling height for each horizon was set to 4 cm. It is hard for Cr to migrate in soil from Zhuzhou on account of the strong Cr retention capacity in the upper soil Z1. The height of the upper soil was thus set to 2 cm with a filling height of 6 cm for subsoil Z2 to ensure that the Cr in the effluent could reach the breakthrough point within a suitable experimental period. The pre-saturation process, settings for experimental parameters and water samples collection procedure were consistent with homogeneous columns. As for the solid phase, soils were excavated by 2 cm increments (4 fractions in total for each column) after the transport experiments.

The collected water samples and soil samples were then used for total Cr/Cr(VI) concentration analysis. The concentration of Cr(III) was further calculated as Eq. (1). Total Cr in effluents was detected by means of an inductively coupled plasma optical emission spectrometer (iCAP PRO, Thermo Scientific, USA). The concentration of Cr(VI) was measured by a UV spectrophotometer (WFJ2-7200, Unico (Shanghai) Instruments Co., Ltd., China) after chromogenic reaction with 1,5-diphenyl carbonize (Zhao et al., 2009). Soil samples were digested by HCl-HNO_3-H_2O_2 in a full-automatic microwave (Topwave, Analytic Jena, Germany) for total Cr determination (Gaudino et al., 2007). The concentration of Cr(VI) in soil was determined by the alkaline extraction method (Fu et al., 2017). For quality control, soil reference material (CRM036) was used and the recoveries of elements were 95.6–103.8 % when compared with the certified values.

$$\mathrm{Cr(III)} = \mathrm{Total\ Cr} - \mathrm{Cr(VI)} \tag{1}$$

2.3. Numerical modeling

A numerical model which can precisely describe Cr migration and transformation during the experiments was constructed, and the calibrated parameters could be further used for long-term migration. The reactive transport model was coupled with a saturated water flow model and a solute transport model in porous media, and the specific coupling process is as described below.

2.3.1. Saturated water flow model

The porous media and fluid were homogenized into a single medium for the modeling simplification. Darcy's law with continuity equation was applied to describe the water moving in an aquifer.

$$\frac{\partial}{\partial t}(\rho\theta) + \nabla\cdot(\rho u) = Q_m \tag{2}$$

In the above equation, ρ (kg/m^3) is the fluid density, θ denotes the porosity which is defined as the fraction of the control volume that is occupied by pores, u (m/s) is the Darcy flow rate, and Q_m (kg/(m^3·s)) represents the mass source (positive) or sink (negative) term.

The velocity field is determined by the pressure gradient, the fluid viscosity, and the structure of the porous medium.

$$u = -\frac{K_S}{\rho g}\nabla P \tag{3}$$

where Ks (m/s) is the hydraulic permeability of the porous medium, g (m^2/s) is the vector of gravitational acceleration, and P (Pa) denotes the pore pressure.

2.3.2. Solute transport model

Combined with a convection-dispersion equation that governs the physical process of solute transport, solute adsorption and redox reactions were also coupled in the reactive solute transport model. This model could be written as:

$$\frac{\partial c_i}{\partial t} + \nabla\cdot J_i + u\cdot\nabla c_i = R_i \tag{4}$$

where c_i (mol/m^3) is the concentration of the solute species, J_i (mol/(m^2·s)) denotes the mass flux diffusive flux vector, u (m/s) is the mass averaged velocity vector, and R_i (mol/(m^3·s)) is the reaction rate expression for the species.

J_i is defined as follows:

$$J_i = -D_i\nabla c_i \tag{5}$$

where D_i (m^2/s) denotes the diffusion coefficient which could be obtained via tracing experiments (Text S1).

The Langmuir adsorption isotherm was used to generalize the solute adsorption process:

$$c_P = c_{Pmax}\frac{K_L c}{1 + K_L c} \quad (6)$$

where c_p (mol/kg) is the adsorption capacity at a given time, c_{pmax} (mol/kg) represents the adsorption capacity, K_L (m^3/mol) is Langmuir constant, and c (mol/m^3) denotes the solute concentration in the liquid phase at a given time.

A reaction network model was constructed to describe the redox process of Cr(III)/Cr(VI) (Text S2). Input parameters were calibrated according to the distribution of Cr species in the solid/liquid phase and used for long-term prediction (Texts S3 and S4).

3. Results and discussion

3.1. Soil properties

The soil properties varied significantly with regions and burial depth (Table 1). The topsoils in the three sites were silt loam with silt particles accounting for over 50 %, whereas the subsoils in Shijiazhuang and Guangzhou were sandy loam with larger soil aggregates. Soils from Shijiazhuang and Guangzhou had slight alkaline pH values (8.4 ± 0.2 and 7.4 ± 0.1, respectively), while the soils in Zhuzhou were acidic with a pH value of 4.8 ± 0.3. The DOC concentrations in the topsoil of the three sites were higher than those in the deep soil, which was probably related to the greater proportion of silt (Laegdsmand et al., 2005). The soil samples exhibited a wide range of cation exchange capacity (CEC), ranging from 3.63 cmol/kg to 33.65 cmol/kg. The contents of Fe and Mn in Zhuzhou soil (Fe: 86.15 ± 13.40 mg/g, Mn: 0.64 ± 0.11 mg/g) were about two to three times of those in Shijiazhuang (Fe: 27.43 ± 0.16 mg/g, Mn: 0.33 ± 0.06 mg/g) and Guangzhou sites (Fe: 32.68 ± 1.30 mg/g, Mn: 0.28 ± 0.04 mg/g). Soils in Shijiazhuang and Guangzhou had a rather low background Cr value (50– 70 mg/kg), while the Cr content in the Zhuzhou site was up to 125.1 mg/kg. Background Cr in all sites was mainly present in the form of stable Cr(III) with poor mobility. According to the field investigation, lead was highly accumulated in the soil of the Zhuzhou site, which exceeded the national standard by about 40 times. X-ray diffraction (XRD) analysis showed that the main crystalline components in H1 soil contain gypsum, hewellite, anglesite, quartz, plumbojarosite and galena (Supplementary Information Fig. S3). Overall, the characteristics of the selected soil samples differed largely from each other, which may affect the migration and transformation of Cr.

3.2. Transport and transformation of Cr(VI) in saturated soil columns

3.2.1. Breakthrough curves of Cr(VI) transport

The BTCs of Cr(VI) in columns filled with different soils are shown in Fig. 1. For soils from Shijiazhuang, C/C_0 of Cr(VI) rapidly reached the peak after 4 PVs in both soil horizons (Fig. 1a). In spite of 1 PV delay in the breakthrough point, the BTCs of Cr(VI) in the subsoil achieved a stable breakthrough platform faster than that in the topsoil. This may be due to the high dispersion coefficient of H1 soil (D = 7.84 cm^2/h), which leads to a stronger solute diffusion effect during the migration process. Compared with the high mobility of Cr(VI) in the Shijiazhuang site, the transport of Cr in the Zhuzhou site was obviously inhibited. During the experiment, up to 120 PVs of Cr(VI) solution were injected into the soil column with no Cr (VI) detected in the effluent of the Z1 soil column. Cr(VI) in Z2 effluent was detected after 80 PVs, and the maximum C/C_0 value reached 64 % after 120 PVs. The results above implied that Cr had a greater migration tendency in the subsoil of Zhuzhou site than in the topsoil. A similar pattern of soil horizon differences in Cr mobility was also verified in the Guangzhou site. As shown in Fig. 1c, the transport and diffusion of Cr(VI) in the G2 soil column slowed down over time. Compared to G2, the breakthrough point of G1 was about 4 PVs earlier and peaked at approximately 7 PVs, which demonstrated the faster transport and diffusion of Cr(VI) in G1. In general, Cr(VI) in Shijiazhuang and Guangzhou samples had a greater mobility than in Zhuzhou soil.

The observed differences in the mobility of Cr(VI) can be ascribed to the soil properties. Cr has a stronger mobility in the soil of the Shijiazhuang site, which may be related to the alkaline soil. On the one hand, the generated negative charges on the soil surface under alkaline conditions could enhance the electrostatic repulsion between Cr(VI) and the soil (Jardine et al., 2013; Xie et al., 2015). On the other hand, an alkaline soil environment would inhibit the formation of hydrogen bonds between $HCrO_4^-$ and $FeO(OH)/Al_2O_3$, thus resulting in less specific adsorption (Liang et al., 2021; Richard and Bourg, 1991). This is also due to the mechanical

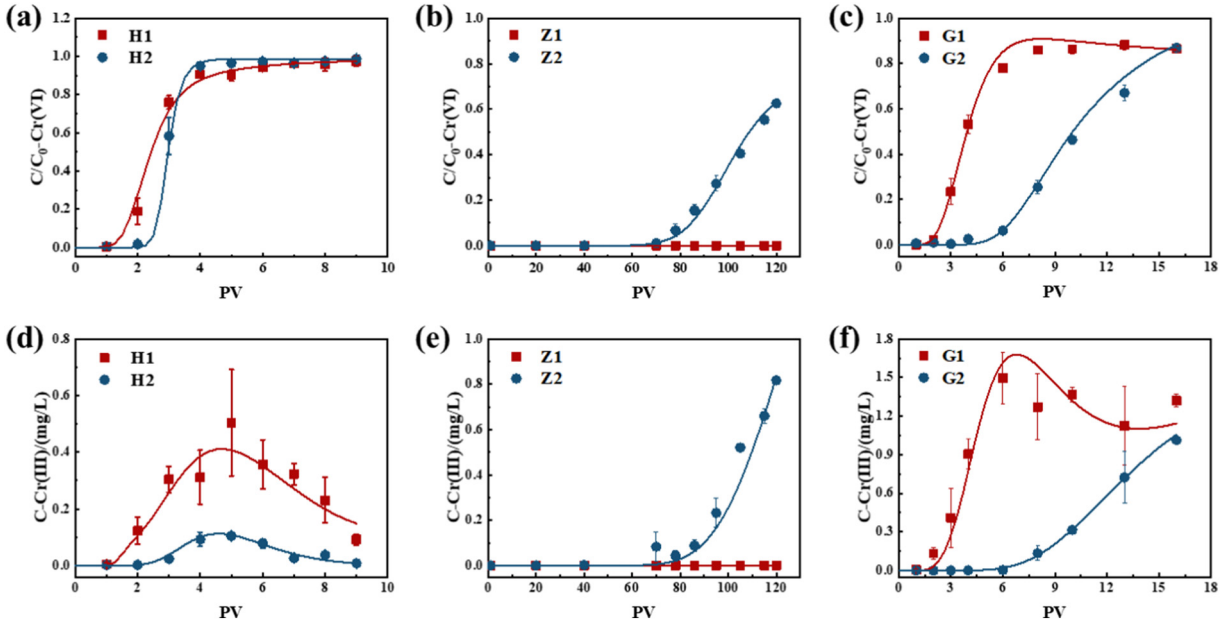

Fig. 1. Breakthrough curves of Cr(VI) and Cr(III) in one-dimensional soil columns filled by soils from different industrial sites with different depths: (a) and (d) Shijiazhuang; (b) and (e) Zhuzhou; (c) and (f) Guangzhou. Each data point represents the mean of three replicates with standard errors at each time point. The symbols represent the experimental results and the solid lines are plotted by simulating results with transport model.

composition of Shijiazhuang soil. The subsoil in Shijiazhuang consisted mainly of coarse-grained sand (Table 1) with a high connectivity density, which is conducive to the formation of preferential flow and makes solute transport in soil less impeded (Pei et al., 2021). Besides, studies have shown that TOC can facilitate the adsorption of Cr(VI) on Fe and Al oxides (Choppala et al., 2018; Tumolo et al., 2020). DOC in soil solution can also act as a carrier of Cr through complexation, ultimately leading to a large number of Cr being retained in soils (Quenea et al., 2009). With less TOC and more DOC, the conditions are more favorable for Cr(VI) migration in G1 (TOC: 29.67 mg/g, DOC: 102.18 mg/kg) than in G2 (TOC: 34.35 mg/g, DOC: 97.50 mg/kg). Moreover, the higher Fe content in G2 (33.48 mg/L) can provide more sites for Cr(VI) adsorption (Khaodhiar et al., 2000). This also contributes to the higher maximum adsorption capacity of G2 (0.009 mol/kg) than that of G1 (0.001 mol/kg). The migration ability of Cr(VI) was strongly inhibited in Zhuzhou soil. In this case, the surface of the Fe and Al oxides became positively charged in the acidic environment, hence promoting the adsorption of Cr(VI) anions. Similarly, the Fe content in soils from Zhuzhou (72.80– 99.49 mg/g) was significantly higher than the Fe content in soils from other regions (27.27– 33.48 mg/g), which provided more specific adsorption sites for Cr(VI). An abnormal inhibition of the transport of Cr(VI) in Z1 with the higher pH value and decreased TOC content compared to Z2 was observed, which could be attributed to the formation of insoluble chromate $PbCrO_4$ (Liang et al., 2021). It is known that Pb^{2+} in the liquid phase reacts preferentially with CrO_4^{2-} due to the low solubility constant ($k_{sp} = 2.8 \times 10^{-13}$ mol^2/L^2) of $PbCrO_4$. $PbCrO_4$ precipitation can also be formed as long as the dissolved Pb^{2+} reaches a concentration of 1.47×10^{-12} mol/L. According to a previous site survey, high concentrations of Pb were detected in Z1 soil, which made it possible to form $PbCrO_4$ precipitation (Table 1).

To verify our hypothesis, XRD and SEM-EDS analyses were performed. The peak for $PbSO_4$ in the Z1 sample after column experiments was reduced compared with the peak in the original samples, indicating the dissolution of $PbSO_4$ during migration. Also, the observation of a $PbCrO_4$ peak verified the formation of $PbCrO_4$ precipitation (Fig. S3). SEM-EDS results further provided direct evidence to explain the mechanism of Cr retention in soil. As shown in Figs. S4 and S5, soil minerals mostly formed irregularly shaped grains composed of octahedral crystals, where $PbSO_4$ partially dissolved. Moreover, the chemical composition of the analyzed particles showed that Pb, S, O and Cr co-existed in the soil grains (Fig. S5), and their ratios corresponded to the elemental composition of $PbCrO_4$ and $PbSO_4$. Thus, it is likely that the dissolution process of $PbSO_4$ was accompanied by the formation of $PbCrO_4$. This observation further confirmed our hypothesis that the formation of $PbCrO_4$ impeded Cr(VI) migration.

3.2.2. REDOX processes of Cr during transport

The amount of Cr(III) in the effluents was also detected so as to describe the reduction process during the migration of Cr(VI). The BTCs of Cr(III) in different soils also showed great differences. Generally, the reduction ability of the soils for Cr(VI) followed the order of Guangzhou > Shijiazhuang > Zhuzhou. For the Shijiazhuang site, the effluent concentration of Cr(III) in H1 was significantly higher than that in H2. Effluent Cr(III) concentrations in two soils went through a gradual increase to a maximum concentration at 4– 5 PVs, followed by a stable decline over time (Fig. 1d). No Cr(III) was detected in the effluent of Z1 during the experiment, while Cr(III) in Z2 soil column was detected as of approximately 70 PVs (Fig. 1e). In the site of Guangzhou, more Cr(III) flowed out with effluents in G1 in comparison to G2. The concentration of Cr(III) in G1 effluent increased rapidly at 0– 6 PVs, and then began to decline after 6 PVs. Similar to the pattern of Cr(VI), the concentration of Cr(III) in G2 effluent slowly climbed from 6 PV until the end of the experiment (Fig. 1f).

To further explain the change of the Cr(III) concentration in effluent, we calculated the retention of Cr(VI) and Cr(III) in the solid phase based on the constructed reactive solute transport model (Fig. 2). As can be seen in Figs. 1 and 2, the accumulation of Cr(VI)/Cr(III) in soil was highly associated with their concentration in the liquid phase given that an equilibrium adsorption model was coupled. It can be concluded that the total Cr retention in the Zhuzhou site was significantly higher than in the Guangzhou and Shijiazhuang sites. Fe oxides can effectively adsorb Cr(VI) in pore water, thus resulting in the retention of Cr(VI) in the solid phase (Johnston and Chrysochoou, 2014). Lower Fe contents in Shijiazhuang soil contributed to the decreased adsorption of Cr(VI) on the specific adsorption sites (Table 1), which can be used to explain the lowest amount of retained Cr(VI) in Shijiazhuang soil. As shown in Fig. 1a and d, changes of the Cr(III) concentration in the effluent were into correspondence with the penetration process of Cr(VI). Before Cr(VI) reached the breakthrough plateau, more reactants were available for the reduction process, which led to an increase of the Cr(III) concentration. When the retained Cr(VI) reached the maximum adsorption capacity of the soil, the concentration of Cr(VI) in the liquid phase tended to stabilize. However, the reduction of Cr(VI) could be inhibited with Fe(II) and organic matter continuously being

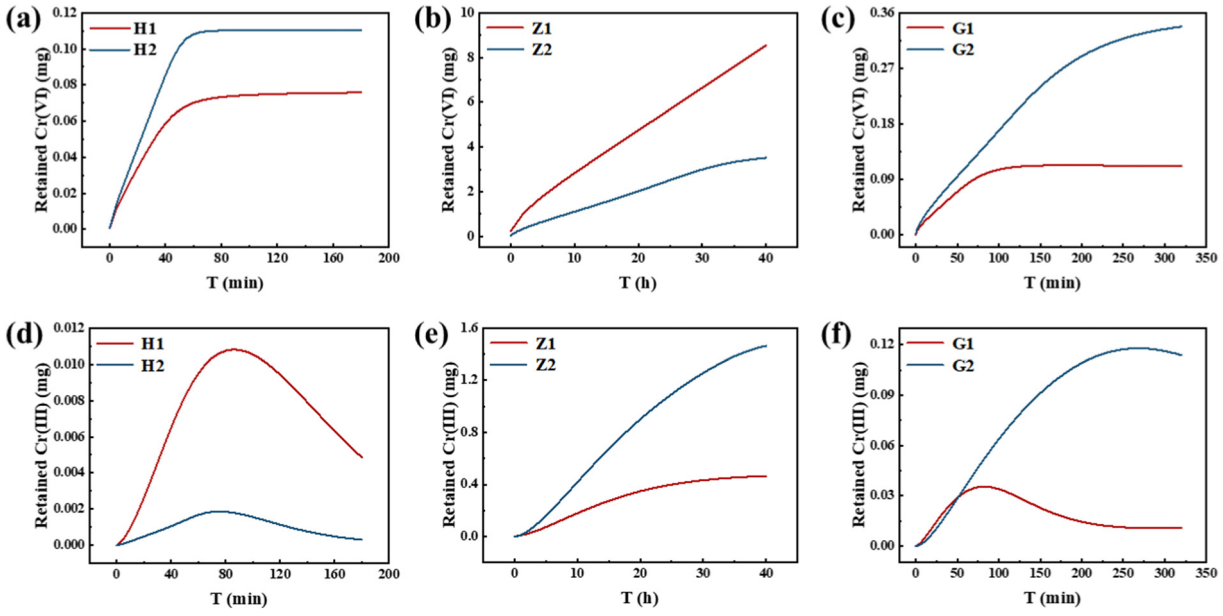

Fig. 2. The retention increments of Cr(VI) and Cr(III) over time during column experiments simulated by transport model in different industrial sites with various soil depths: (a) and (d) Shijiazhuang; (b) and (e) Zhuzhou; (c) and (f) Guangzhou.

washed out. With the on-going leaching of Cr(III) in the liquid phase, the concentration gradient between soil solutions and soil particles led to the re-dissolution of adsorbed Cr(III) in the solid phase, further causing a decrease in solid accumulation (Fig. 2a and d). The retained Cr(III) in Z2 was significantly higher than in Z1 (Fig. 2b and e), indicating that the subsoil had a greater reduction capacity for Cr(VI) in Zhuzhou. In an acidic environment, Cr(VI) presents a strong oxidation capacity with a high redox potential (Dong et al., 2020). Therefore, Cr(VI) is more easily reduced to Cr(III) in Z2 with a lower pH. As discussed in Section 3.2.1, once injected into the soil column, dissolved Cr(VI) could co-precipitate with Pb to stable $PbCrO_4$, which inhibited the reaction with reducing substances (Fe, DOC, etc.) in the topsoil. In addition, Cr(III) in Z2 could readily combine with hydroxide and sulphate to form insoluble chelates or react with OM and soil colloids to form precipitates, thus remaining at a higher concentration in soils (Ao et al., 2022a). As for the Guangzhou site, the distribution of Cr(III) between the solid-liquid phase for G1 exhibited the same trend as in the Shijiazhuang site. In spite of the lower amount of Cr(III) in the effluent, more Cr(III) was retained in G2 soil compared to G1, suggesting stronger Cr(VI) reduction in the subsoil (Fig. 2f). This can be explained by the high organic matter content in G2 soil, which facilitates the transfer of electrons from biometabolites to Cr(VI) by driving microbial growth, and further promoting the redox transformation of Cr(VI) (Thacher et al., 2015). Besides, the higher adsorption capacity of Cr(III) in G2 soil (0.039 mol/kg) also contributed to this accumulation in the solid phase.

3.2.3. Correlation analysis between transport parameters and control factors

In order to identify the main controlling factors of Cr(VI) migration and transformation in soil, correlation analysis was conducted on typical migration and transformation parameters and representative soil physicochemical properties. As shown in Fig. 3, Fe content and pH value were the major factors controlling the fate of Cr(VI). The Fe content in soil significantly positively impacted the adsorption and reduction process of Cr(VI) ($r = 0.949$, $p < 0.01$). This result was consistent with the findings of Yang et al. (2022) that Fe minerals played an important role in Cr(VI) reduction. Soil pH could control the transport behavior of Cr by affecting soil chemical and mineralogical properties and the solubility of natural OM and competing oxygen anions (Ao et al., 2022a; Xu et al., 2020). Analytical results showed that the pH was negatively correlated with the

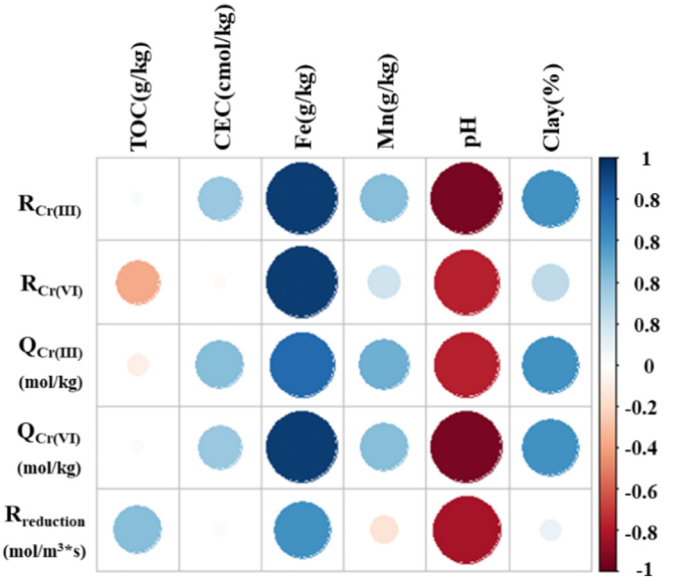

Fig. 3. Analysis of the correlation between transport parameters and soil physicochemical properties ($R_{Cr(III)}$: retardation factor of Cr(III) in soil columns; $R_{Cr(VI)}$: Retardation factor of Cr(VI) in soil columns; $Q_{Cr(III)}$: maximum adsorption of Cr(III) in soil columns; $Q_{Cr(VI)}$: maximum adsorption of Cr(VI) in soil columns; $R_{reduction}$: average reduction rate of Cr(VI) during transport).

adsorption of Cr(VI) ($r = -0.909$, $p < 0.05$), which is in line with previous studies (Rouhaninezhad et al., 2020; Yolcubal and Akyol, 2007). With the increase of pH, the adsorption of Cr(VI) by soil mineral particles showed a decreasing trend. In terms of other factors, the adsorption capacity of Cr increases with CEC and clay content ($r = 0.867$, $p < 0.05$). Additionally, TOC and Mn content also have a slight effect on the redox process. The reduction rate of Cr(VI) was positively correlated with the TOC content, indicating the potential impact of organic matter on Cr(VI) reduction. Yet, the Mn content was negatively correlated with the reduction rate of Cr(VI) owing to its oxidizability (Dai et al., 2011). It has been shown that Mn oxides can substantially promote Cr(III) oxidation through internal electron transfer (Hausladen and Fendorf, 2017).

3.3. Long-term simulation and risk evaluation of Cr(VI) transport in soil profile

In order to simulate the vertical migration and transformation process of Cr(VI) in vertical heterogeneous media, additional migration experiments were conducted in multi-horizon soil systems. Based on the results, we further optimized the migration model to achieve an accurate simulation in soil profile. According to Figs. 4 and S6, the fitted values of the Cr(VI) concentration in the effluent and in the solid phase obtained from the migration model agreed reasonably with the measured experimental results in this study. The migration and transformation of Cr(VI) in the heterogeneous soil profile of three sites are similar to the experimental results of homogeneous soils. Cr(VI) still showed the strongest mobility and oxidizing capacity in the Shijiazhuang site (Fig. 4a and c). Higher OM content and lower pH promoted the adsorption of Cr(VI) by Fe and Al oxides (Choppala et al., 2018), which can explain the increase of Cr(VI) retention in the topsoil (Fig. S6a). Although the adsorption of Cr(VI) reached an equilibrium, the retention of Cr(III) in the solid phase presented an upward trend. This phenomenon mainly stems from the fact that the concentrations of Fe(II) and OM in the model remain constant, thus providing a stable source of reduction reactants at the site scale. In addition, the generated Cr(III) would be retained in the solid phase due to the high adsorption capacity of the soils (Table 2), resulting in the reduction of the reaction products in the soil solution, which further leads to the progress of the reduction reactions. In the Zhuzhou site, Cr(VI) was detected in the effluent after 850 PVs, while BTCs did not reach the breakthrough plateau ultimately (Fig. 4b), which corresponded to large Cr(VI) retention in the soil near the column inlet (Fig. S6b). In addition, no Cr(III) was basically tested in the effluent (Fig. 4d). From these results, it is clear that Cr(VI) reduction hardly took place and Cr migration was hindered to some extent. Compared with Fig. 1c, the Cr(VI) transport rate in stratified soil columns of the Guangzhou site is in between the transport rates in homogeneous G1 and G2 soil columns (Fig. 4a). Concentrations of Cr(III) in the effluent were basically elevated with the increase of the Cr(VI) concentration due to the progress of the reduction reaction (Fig. 4c).

On account of the site migration parameters obtained (Table 2), the long-term migration risk of Cr(VI) in Shijiazhuang, Zhuzhou and Guangzhou sites was predicted for a period of 20 years under the condition of Cr residues leaching (Text S4). The dynamic distribution of the Cr(VI) and Cr(III) contents in the solid-liquid phase is shown in Fig. 5. From the long-term prediction results of the Shijiazhuang site, the distribution of Cr(VI) in the solid-liquid phase reached equilibrium under heavy rainfall conditions within 10 years and the pollution could spread to depths of 6 m. This is because the high sand content in Shijiazhuang soil creates proper conditions for vertical migration of Cr to the deep soil. Moreover, the Cr(VI) concentration in the liquid phase could reach 10 ppm within the simulation period and thus poses a threat to the subsoil and the groundwater. Compared with the heavy rainfall scenario, the leaching of Cr(VI) under a scenario of weak rainfall caused less hazard to the soil and the groundwater due to lower Cr(VI) infiltration into the system (Fig. 5). Besides, the smaller Darcy velocity in weak rainfall conditions would weaken solute convection and diffusion (Akhtar et al., 2011). As for Cr(III), the concentration distribution in the solid/liquid phases exhibited the same pattern under the two boundary conditions. It is worth noting that the total amount of Cr(III)

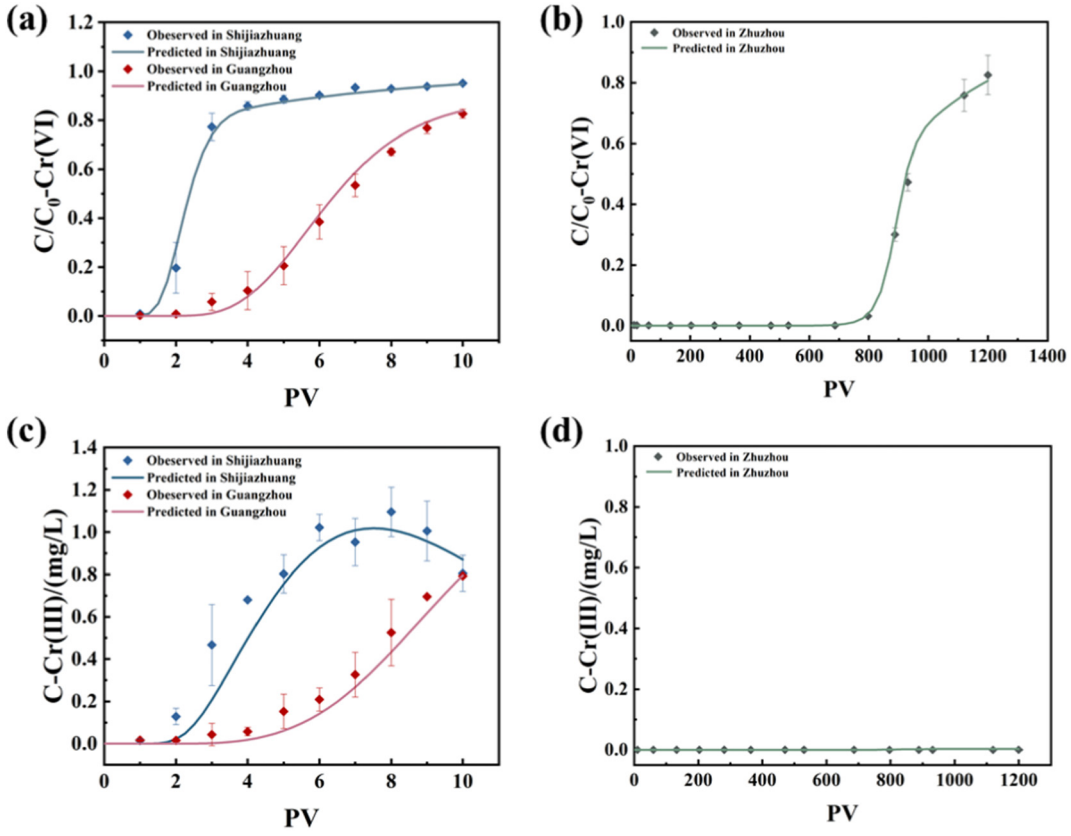

Fig. 4. Breakthrough curves of Cr(VI) and Cr(III) in the soil profile (Shijiazhuang, Zhuzhou, and Guangzhou). Each data point represents the mean of three replicates with standard errors at each time point. The symbols represent the experimental results and the solid lines are plotted by simulating results with multidimensional transport model.

retained in the topsoil was higher with the leaching effect of weak rainfall than that under the condition of heavy rainfall within 20 years. The result may be attributed to a longer contact time between Cr(VI) and reducing substances (OM, Fe and Mn oxides) in the soil solution under weak rainfall, so that more reduction products of Cr(III) were formed. Cr(VI) leakage was immobilized in the topsoil under both rainfall conditions in the Zhuzhou site (Fig. 5) due to $PbCrO_4$ precipitation, thus posing a low degree of diffusional risk. Similar to Shijiazhuang, rainfall intensity also produced a significant effect on the vertical migration risk posed by Cr(VI) in the Guangzhou site (Fig. 5), which is consistent with the studies of Pedrot et al. (2008) and Wei et al. (2021). Rainfall could control the processes and diffusion on pollutant transport in soil (Gao et al., 2004). As the maximum adsorption capacity of Cr(VI) in G1 ($9E^{-4}$ mol/kg) was far smaller than that in G2 ($9E^{-3}$ mol/kg), Cr(VI) was mostly accumulated in the deep soil with a concentration up to $2.5E^{-4}$ mol/kg within 20 years. As a whole, the soil Cr(VI) pollution posed a high ecology risk in Guangzhou site. Besides, the anaerobic environment with low Eh promoting the conversion of Cr(VI) to Cr(III) and decreasing the effective diffusion of Cr (Zhang and Lin, 2020). The strongest reduction ability of Cr(VI) was observed in the Guangzhou soil, which gradually retained increasing amounts of Cr(III) over time. Prediction results demonstrated that the Cr(III) concentration in the liquid phase of the subsoil could reach 0.08 mol/m^3 within 20 years. A large amount of Cr(VI) was reduced by reductive materials, further causing the decrease of the Cr(VI) content in the liquid phase of the subsoil. The speciation of Cr plays an important part in regulating the transport behavior of Cr(VI). Hence, it can be inferred that morphological transformation of Cr(VI) should also be taken into account when predicting Cr(VI) migration risk.

Table 2
Fitted parameters of Cr transport and transformation in multi-horizon columns.

Parameters[a]	H1	H2	Z1	Z2	G1	G2
k1 (L/(mol·s))	2	2	5	5	4	4.5
k2 (L/(mol·s))	1	1	0.5	0.5	0.5	0.5
k3 (L/(mol·s))	0.2	0.2	0.2	0.2	0.2	0.2
K_L Cr(VI) (m^3/mol)	1.5	1.4	5	8	0.9	0.4
c_{pmax} Cr(VI) (mol/kg)	6E−4	5.5E−4	0.4	5E−2	9E−4	9E−3
K_L Cr(III) (m^3/mol)	2	1.8	1	0.9	1.5	0.45
c_{pmax} Cr(III) (mol/kg)	1.9E−3	1.41E−3	0.5	0.1	1.5E−2	2.1E−2

[a] k1 is the rate constant of Cr(VI) consumption by Fe(II) for Cr(III) generation; k2 is the rate constant of Cr(VI) consumption by OrgI for Cr(III) generation; k3 is the rate of Cr(III) consumption for Cr(VI) generation; K_L is Langmuir constant; c_{pmax} represents the adsorption capacity.

4. Conclusion

In this study, column experiments were conducted on the migration and transformation of Cr(VI) in different soil horizons and sites. The multi-process coupling model of Cr transformation and migration was established to simulate the fate of Cr(VI) in homogeneous and longitudinal heterogenic soil systems. The alkaline soils in Shijiazhuang provided a suitable environment for Cr(VI) transport in both soil horizons. In Zhuzhou site, a large amount of Cr(VI) was retained in the topsoil due to the formation of $PbCrO_4$. Differences in Cr mobility between soil horizons were observed in the Guangzhou site. The transport of Cr(VI) was faster in the Guangzhou upper soil, while the retarding ability of Cr(VI) in the subsoil is strong owing to high TOC and Fe content. Through correlation analysis between key soil properties and model parameters, it was found that pH and Fe content were the main controlling factors on Cr(VI) migration and transformation. Long-term prediction of the site conceptual model showed that the ecological risk of Cr(VI) follows the order of Guangzhou > Shijiazhuang > Zhuzhou. In the simulation process, rainfall intensity significantly affected the migration and diffusion behavior of Cr(VI). Heavy rainfall would bring greater vertical transport risk, while weak rainfall conditions were more conducive to the reduction of Cr(VI). Overall, the outcome of this work

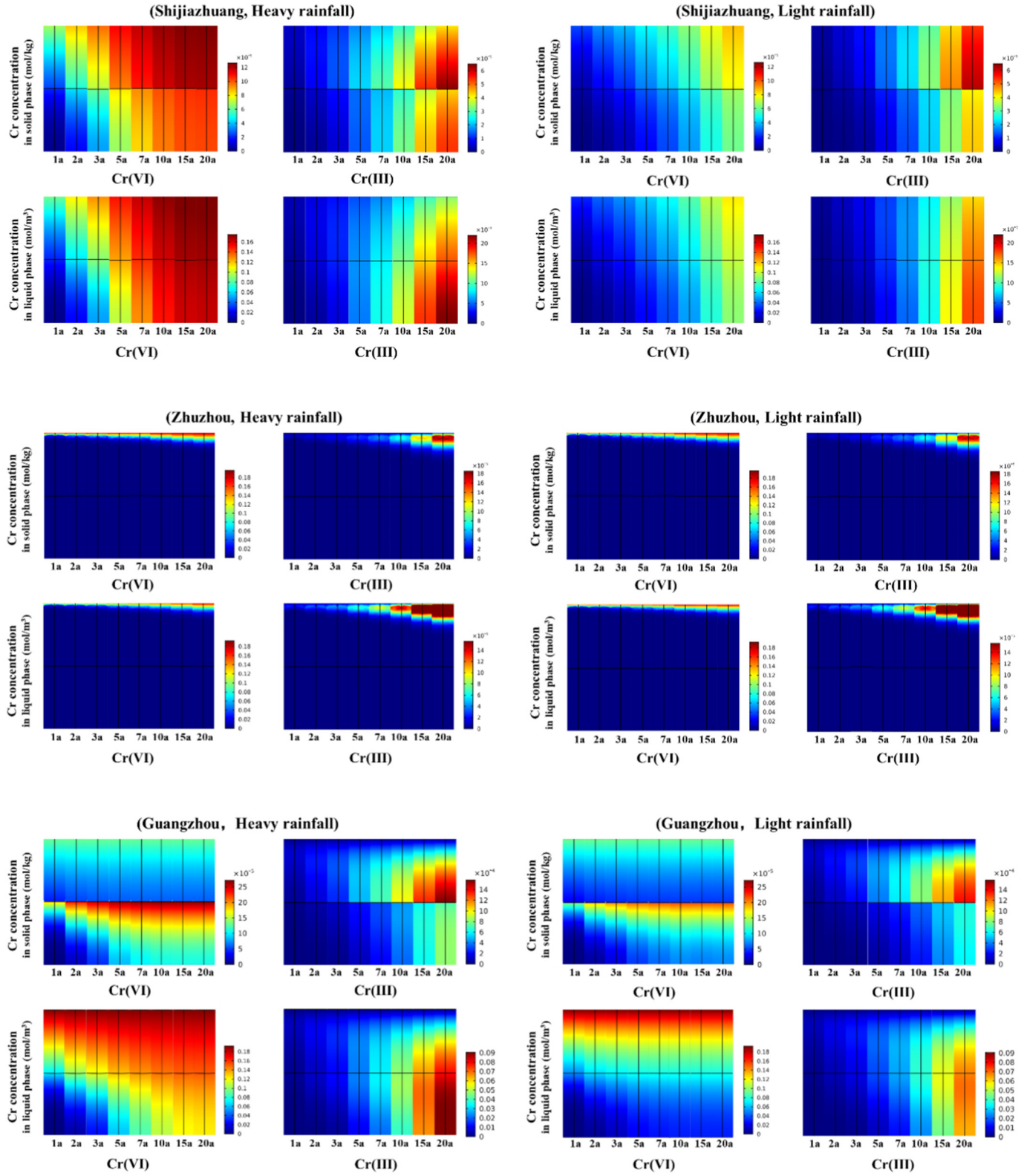

Fig. 5. The long-term simulation results of Cr(VI) transport in the Shijiazhuang, Zhuzhou, and Guangzhou sites for a period of 20 years under heavy and light rainfall conditions. The concentrations of Cr were expressed as mol/kg in the solid phase and mol/m^3 in the liquid phase.

contributes to comprehensively understanding of the environmental fate and transport of Cr at a wider vertical scale and provides evidence-based strategies for the remediation of industrial sites. Specially, the longitudinal heterogeneity of the soil was considered in the model construction, which could produce a more precise prediction for the long-term risks in Cr-contaminated sites. Besides, the good match between experimental results and simulated BTCs of Cr indicates successful applicability of the transport model for the three sites. Furthermore, the horizontal migration of pollutants caused by groundwater will also lead to the diffusion of heavy metal pollution in soils. Further studies are recommended to focus

on the transport and ecological risk of Cr migration under the complex conditions of multi-dimension and multi-medium in the actual sites.

CRediT authorship contribution statement

Xuchen Yan: Investigation, Formal analysis, Writing – original draft. **Bin Yang:** Data curation, Writing – review & editing. **Erkai He:** Writing – review & editing, Funding acquisition. **Willie J.G.M. Peijnenburg:** Writing – review & editing. **Ling Zhao:** Writing – review & editing. **Xiaoyun Xu:** Writing – review & editing. **Xinde Cao:** Writing – review & editing, Project administration. **Ana Romero-Freire:** Writing – review & editing. **Hao Qiu:** Conceptualization, Supervision, Writing – review & editing, Funding acquisition.

Data availability

Data will be made available on request.

Declaration of competing interest

The authors declare that they have no known competing financial interests or personal relationships that could have appeared to influence the work reported in this paper.

Acknowledgements

This study was supported by the National Key Research and Development Program of China (No. 2020YFC1808000, No. 2018YFC1800600).

Appendix A. Supplementary data

Supplementary data to this article can be found online at https://doi.org/10.1016/j.scitotenv.2022.159799.

References

Akhtar, M.S., Stuben, D., Norra, S., Memon, M., 2011. Soil structure and flow rate-controlled molybdate, arsenate and chromium(III) transport through field columns. Geoderma 161, 126–137.

Ao, M., Chen, X.T., Deng, T.H.B., Sun, S.S., Tang, Y.T., Morel, J.L., et al., 2022a. Chromium biogeochemical behaviour in soil-plant systems and remediation strategies: a critical review. J. Hazard. Mater. 424, 127233.

Ao, M., Sun, S., Deng, T., Zhang, F., Liu, T., Tang, Y., et al., 2022b. Natural source of Cr(VI) in soil: the anoxic oxidation of Cr(III) by mn oxides. J. Hazard. Mater. 433, 128805.

Bai, J.H., Xiao, R., Cui, B.S., Zhang, K.J., Wang, Q.G., Liu, X.H., et al., 2011. Assessment of heavy metal pollution in wetland soils from the young and old reclaimed regions in the Pearl River estuary, South China. Environ. Pollut. 159, 817–824.

Balkhair, K.S., 2017. Modeling fecal bacteria transport and retention in agricultural and urban soils under saturated and unsaturated flow conditions. Water Res. 110, 313–320.

Banks, M.K., Schwab, A.P., Henderson, C., 2006. Leaching and reduction of chromium in soil as affected by soil organic content and plants. Chemosphere 62, 255–264.

Chen, H.X., Dou, J.F., Xu, H.B., 2018. Remediation of Cr(VI)-contaminated soil with co-composting of three different biomass solid wastes. J. Soils Sediments 18, 897–905.

Chen, M., Tao, X.Y., Wang, D.J., Xu, Z.B., Xu, X.Y., Hu, X.F., et al., 2019. Facilitated transport of cadmium by biochar-Fe3O4 nanocomposites in water-saturated natural soils. Sci. Total Environ. 684, 265–275.

Choppala, G., Kunhikrishnan, A., Seshadri, B., Park, J.H., Bush, R., Bolan, N., 2018. Comparative sorption of chromium species as influenced by pH, surface charge and organic matter content in contaminated soils. J. Geochem. Explor. 184, 255–260.

Coetzee, J.J., Bansal, N., Chirwa, E.M.N., 2020. Chromium in environment, its toxic effect from chromite-mining and ferrochrome industries, and its possible bioremediation. Exp. Health 12, 51–62.

Dai, R.N., Yu, C.Y., Gou, J., Lan, Y.Q., Mao, J.D., 2011. Photoredox pathways of Cr(III)-tartrate complexes and their impacting factors. J. Hazard. Mater. 186, 2110–2116.

del Real, A.E.P., Perez-Sanz, A., Garcia-Gonzalo, P., Castillo-Michel, H., Gismera, M.J., Lobo, M.C., 2020. Evaluating cr behaviour in two different polluted soils: mechanisms and implications for soil functionality. J. Environ. Manag. 276, 111073.

Dinter, T.C., Gerzabek, M.H., Puschenreiter, M., Strobel, B.W., Couenberg, P.M., Zehetner, F., 2021. Heavy metal contents, mobility and origin in agricultural topsoils of the Galapagos Islands. Chemosphere 272, 129821.

Dong, H., Wei, G., Cao, T., Shao, B., Guan, X., Strathmann, T.J., 2020. Insights into the oxidation of organic cocontaminants during Cr(VI) reduction by sulfite: the overlooked significance of Cr(V). Env. Sci. Tech. 54, 1157–1166.

Fu, R.B., Wen, D.D., Xia, X.Q., Zhang, W., Gu, Y.Y., 2017. Electrokinetic remediation of chromium (Cr)-contaminated soil with citric acid (CA) and polyaspartic acid (PASP) as electrolytes. Chem. Eng. J. 316, 601–608.

Gao, B., Walter, M.T., Steenhuis, T.S., Hogarth, W.L., Parlange, J.Y., 2004. Rainfall induced chemical transport from soil to runoff: theory and experiments. J. Hydrol. 295, 291–304.

Gaudino, S., Galas, C., Belli, M., Barbizzi, S., de Zorzi, P., Jacimovic, R., et al., 2007. The role of different soil sample digestion methods on trace elements analysis: a comparison of ICP-MS and INAA measurement results. Accred. Qual. Assur. 12, 84–93.

Hausladen, D.M., Fendorf, S., 2017. Hexavalent chromium generation within naturally structured soils and sediments. Env. Sci. Tech. 51, 2058–2067.

Izbicki, J.A., Wright, M.T., Seymour, W.A., McCleskey, R.B., Fram, M.S., Belitz, K., et al., 2015. Cr(VI) occurrence and geochemistry in water from public-supply wells in California. Appl. Geochem. 63, 203–217.

Jardine, P.M., Stewart, M.A., Barnett, M.O., Basta, N.T., Brooks, S.C., Fendorf, S., et al., 2013. Influence of soil geochemical and physical properties on chromium(VI) sorption and bioaccessibility. Env. Sci. Tech. 47, 11241–11248.

Jia, M.Q., Bian, X., Yuan, S.H., 2017. Production of hydroxyl radicals from Fe(II) oxygenation induced by groundwater table fluctuations in a sand column. Sci. Total Environ. 584, 41–47.

Johnston, C.P., Chrysochoou, M., 2014. Mechanisms of chromate adsorption on hematite. Geochim. Cosmochim. Acta 138, 146–157.

Khaodhiar, S., Azizian, M.F., Osathaphan, K., Nelson, P.O., 2000. Copper, chromium, and arsenic adsorption and equilibrium modeling in an iron-oxide-coated sand, background electrolyte system. Water Air and Soil Pollut 119, 105–120.

Laegdsmand, M., de Jonge, L.W., Moldrup, P., 2005. Leaching of colloids and dissolved organic matter from columns packed with natural soil aggregates. Soil Sci. 170, 13–27.

Li, B.R., Liao, P., Xie, L., Li, Q.Q., Pan, C., Ning, Z.G., et al., 2020. Reduced NOM triggered rapid Cr(VI) reduction and formation of NOM-Cr(III) colloids in anoxic environments. Water Res. 181, 115923.

Li, F.Y., Fan, Z.P., Xiao, P.F., Oh, K., Ma, X.P., Hou, W., 2009. Contamination, chemical speciation and vertical distribution of heavy metals in soils of an old and large industrial zone in Northeast China. Environ. Geol. 57, 1815–1823.

Liang, J.L., Huang, X.M., Yan, J.W., Li, Y.Y., Zhao, Z.W., Liu, Y.Y., et al., 2021. A review of the formation of Cr(VI) via Cr(III) oxidation in soils and groundwater. Sci. Total Environ. 774, 145762.

Liu, Z.Y., Fei, Y., Shi, H.D., Mo, L., Qi, J.X., 2022. Prediction of high-risk areas of soil heavy metal pollution with multiple factors on a large scale in industrial agglomeration areas. Sci. Total Environ. 808, 151874.

Lov, A., Sjostedt, C., Larsbo, M., Persson, I., Gustafsson, J.P., Cornelis, G., et al., 2017. Solubility and transport of Cr(III) in a historically contaminated soil - evidence of a rapidly reacting dimeric Cr(III) organic matter complex. Chemosphere 189, 709–716.

Megremi, I., Vasilatos, C., Vassilakis, E., Economou-Eliopoulos, M., 2019. Spatial diversity of cr distribution in soil and groundwater sites in relation with land use management in a Mediterranean region: the case of C. Evia and assopos-thiva basins, Greece. Sci. Total Environ. 651, 656–667.

Muthukumaran, K., Beulah, S., 2010. Removal of chromium (VI) from wastewater using chemically activated Syzygium jambolanum nut carbon by batch studies. Urban Environmental Pollution 2011 (4), 266–280.

Namiesnik, J., Rabajczyk, A., 2012. Speciation analysis of chromium in environmental samples. Crit. Rev. Environ. Sci. Technol. 42, 327–377.

Parizanganeh, A., Hajisoltani, P., Zamani, A., 2010. Assessment of heavy metal pollution in surficial soils surrounding Zinc Industrial Complex in Zanjan-Iran. International Conference on Ecological Informatics and Ecosystem Conservation (Iseis 2010) 2, 162–166.

Pedrot, M., Dia, A., Davranche, M., Bouhnik-Le Coz, M., Henin, O., Gruau, G., 2008. Insights into colloid-mediated trace element release at the soil/water interface. J. Colloid Interface Sci. 325, 187–197.

Pei, Y.W., Huang, L.M., Li, D.F., Shao, M.A., 2021. Characteristics and controls of solute transport under different conditions of soil texture and vegetation type in the waterewind erosion crisscross region of China's loess plateau. Chemosphere 273, 129651.

Peng, J.Y., Zhang, S., Han, Y.Y., Bate, B., Ke, H., Chen, Y.M., 2022. Soil heavy metal pollution of industrial legacies in China and health risk assessment. Sci. Total Environ. 816, 151632.

Qiu, H., Lou, Z., Gu, X., Sun, Y., Wang, J., Zhang, W., Cao, X., 2022. Smart 6S roadmap for deciphering the migration and risk of heavy metals in soil and groundwater systems at brownfield sites nationwide in China. Sci. Bull. 67 (13), 1295–1299.

Quenea, K., Lamy, I., Winterton, P., Bermond, A., Dumat, C., 2009. Interactions between metals and soil organic matter in various particle size fractions of soil contaminated with waste water. Geoderma 149, 217–223.

Richard, F.C., Bourg, A.C.M., 1991. Aqueous geochemistry of chromium: a review. Water Res. 25, 807–816.

Rouhaninezhad, A.A., Hojati, S., Masir, M.N., 2020. Adsorption of cr (VI) onto micro- and nanoparticles of palygorskite in aqueous solutions: effects of pH and humic acid. Ecotoxicol. Environ. Saf. 206, 111247.

Sedlazeck, K.P., Höllen, D., Müller, P., Mischitz, R., Gieré, R., 2017. Mineralogical and geochemical characterization of a chromium contamination in an aquifer - a combined analytical and modeling approach. Appl. Geochem. 87, 44–56.

Thacher, R., Hsu, L., Ravindran, V., Nealson, K.H., Pirbazari, M., 2015. Modeling the transport and bioreduction of hexavalent chromium in aquifers: influence of natural organic matter. Chem. Eng. Sci. 138, 552–565.

Tumolo, M., Ancona, V., De Paola, D., Losacco, D., Campanale, C., Massarelli, C., et al., 2020. Chromium pollution in european water, sources, health risk, and remediation strategies: an overview. Int. J. Environ. Res. Public Health 17, 5438.

Wang, X.R., Li, L., Yan, X.H., Meng, X.G., Chen, Y.C., 2020a. Processes of chromium (VI) migration and transformation in chromate production site: a case study from the middle of China. Chemosphere 257, 127282.

Wang, Y.L., Tsou, M.C., Liao, H.T., Hseu, Z.Y., Dang, W., Hsi, H.C., et al., 2020b. Influence of soil properties on the bioaccessibility of cr and ni in geologic serpentine and anthropogenically contaminated non-serpentine soils in Taiwan. Sci. Total Environ. 714, 136761.

Wei, Y.Q., Xu, X.Y., Zhao, L., Chen, X., Qiu, H., Gao, B., et al., 2021. Migration and transformation of chromium in unsaturated soil during groundwater table fluctuations induced by rainfall. J. Hazard. Mater. 416, 126229.

Wu, C.F., Luo, Y.M., Huang, B.A., Zhang, H.B., Wang, H.Y., 2010. Studies on the chromium concentrations in topsoils and subsoils of two rapidly industrialized cities in the Yangtze River Delta in East China. Environ. Earth Sci. 61, 1239–1247.

Xiao, Q., Zong, Y.T., Lu, S.G., 2015. Assessment of heavy metal pollution and human health risk in urban soils of steel industrial city (Anshan), Liaoning. Northeast China. Ecotoxicol. Environ. Saf. 120, 377–385.

Xie, J.Y., Gu, X.Y., Tong, F., Zhao, Y.P., Tan, Y.Y., 2015. Surface complexation modeling of Cr(VI) adsorption at the goethite-water interface. J. Colloid Interface Sci. 455, 55–62.

Xu, T., Nan, F., Jiang, X.F., Tang, Y.L., Zeng, Y.H., Zhang, W.H., et al., 2020. Effect of soil pH on the transport, fractionation, and oxidation of chromium (III). Ecotoxicol. Environ. Saf. 195, 110459.

Yang, B., Qiu, H., Zhang, P.H., He, E., Xia, B., Liu, Y., et al., 2022. Modeling and visualizing the transport and retention of cationic and oxyanionic metals (Cd and Cr) in saturated soil under various hydrochemical and hydrodynamic conditions. Sci. Total Environ. 812, 151467.

Yolcubal, I., Akyol, N.H., 2007. Retention and transport of hexavalent chromium in calcareous karst soils. Turk. J. Earth Sci. 16, 363–379.

Zeng, F.R., Ali, S., Zhang, H.T., Ouyang, Y.B., Qiu, B.Y., Wu, F.B., et al., 2011. The influence of pH and organic matter content in paddy soil on heavy metal availability and their uptake by rice plants. Environ. Pollut. 159, 84–91.

Zhang, W.J., Lin, M.F., 2020. Influence of redox potential on leaching behavior of a solidified chromium contaminated soil. Sci. Total Environ. 733, 139410.

Zhao, X.M., Dong, D.M., Hua, X.Y., Dong, S.F., 2009. Investigation of the transport and fate of Pb, Cd, Cr(VI) and As(V) in soil zones derived from moderately contaminated farmland in northeast China. J. Hazard. Mater. 170, 570–577.

Zhu, H., Bing, H.J., Wu, Y.H., Zhou, J., Sun, H.Y., Wang, J.P., et al., 2019. The spatial and vertical distribution of heavy metal contamination in sediments of the three gorges reservoir determined by anti-seasonal flow regulation. Sci. Total Environ. 664, 79–88.